Ab Initio Study of the Beryllium Isotopes ^{7}Be to ^{12}Be

Shihang Shen,[1,2,3] Serdar Elhatisari,[4,5,6] Dean Lee,[7] Ulf-G. Meißner,[6,3,8,1,*] and Zhengxue Ren[3]
[1]*Peng Huanwu Collaborative Center for Research and Education, International Institute for Interdisciplinary and Frontiers, Beihang University, Beijing 100191, China*
[2]*School of Physics, Beihang University, Beijing 102206, China*
[3]*Institute for Advanced Simulation (IAS-4), Forschungszentrum Jülich, D-52425 Jülich, Germany*
[4]*Interdisciplinary Research Center for Industrial Nuclear Energy (IRC-INE), King Fahd University of Petroleum and Minerals (KFUPM), 31261 Dhahran, Saudi Arabia*
[5]*Faculty of Natural Sciences and Engineering, Gaziantep Islam Science and Technology University, Gaziantep 27010, Turkey*
[6]*Helmholtz-Institut für Strahlen- und Kernphysik and Bethe Center for Theoretical Physics, Universität Bonn, D-53115 Bonn, Germany*
[7]*Facility for Rare Isotope Beams and Department of Physics and Astronomy, Michigan State University, East Lansing, Michigan 48824, USA*
[8]*Tbilisi State University, 0186 Tbilisi, Georgia*

(Received 26 November 2024; revised 20 February 2025; accepted 3 April 2025; published 25 April 2025)

We present a systematic *ab initio* study of the low-lying states in beryllium isotopes from ^{7}Be to ^{12}Be using nuclear lattice effective field theory with the N^{3}LO interaction. Our calculations achieve good agreement with experimental data for energies, radii, and electromagnetic properties. We introduce a novel, model-independent method to quantify nuclear shapes, uncovering a distinct pattern in the interplay between positive and negative parity states across the isotopic chain. By combining Monte Carlo sampling of the many-body density operator with a novel nucleon-grouping algorithm, the prominent two-center cluster structures, the emergence of one-neutron halo, complex nuclear molecular dynamics such as π orbital and σ orbital, emerge naturally.

DOI: 10.1103/PhysRevLett.134.162503

Introduction—Beryllium isotopes are pivotal in nuclear structure studies due to their diverse phenomena, including clustering, halo structures, and the breakdown of conventional shell closures. For instance, ^{7}Be plays a significant role in big bang nucleosynthesis and nuclear astrophysics by influencing the primordial abundances of light elements [1,2]. The unbound ^{8}Be, which decays into two alpha particles with a long lifetime, exemplifies nuclear instability and clustering effects. Moving along the isotopic chain, ^{9}Be and ^{10}Be are renowned for their pronounced molecular-like structures [3]. The neutron-rich ^{11}Be is particularly notable for its ground-state parity inversion and halo structure, challenging traditional shell-model predictions and providing insights into weakly bound systems [4,5]. Similarly, ^{12}Be exhibits the disappearance of the $N = 8$ shell closure, highlighting the role of intruder configurations and shape coexistence [6–9]. These rich and varied phenomena underscore the need for comprehensive theoretical frameworks capable of capturing the complex interplay of clustering, shell evolution, and continuum effects in beryllium isotopes.

A variety of theoretical approaches have been employed to study these isotopes, with significant emphasis on cluster structures, such as antisymmetrized molecular dynamics (AMD) [10,11], fermionic molecular dynamics (FMD) [12], molecular-orbital models [13,14], the Tohsaki-Horiuchi-Schuck-Röpke (THSR) wave function approach [15–17], and other cluster models [18–22]. These methods have effectively captured cluster structures, molecular configurations, and the influence of valence neutrons in beryllium isotopes. See also the recent reviews [23–25]. In parallel, density functional theory has been employed to predict the formation of alpha clusters bonded by excess neutrons, highlighting the significant role of clustering in these systems [26–28]. *Ab initio* methods such as the Gamow shell model [29], Green's function Monte Carlo [30–32], the resonating group method [33], Monte Carlo shell model (MCSM) [34,35], and no-core shell model (NCSM) [4,36–39] have been instrumental in providing a microscopic understanding of nuclear structure, clustering, and reaction dynamics in beryllium isotopes.

Comprehensive reviews have highlighted the importance of clustering phenomena in light nuclei and their impact on nuclear structure, reaction dynamics, and astrophysics [40–44]. These works emphasize the coexistence of cluster and shell-model features in neutron-rich isotopes and

*Contact author: meissner@hiskp.uni-bonn.de

discuss the challenges in fully understanding the underlying mechanisms. While these theoretical methods have significantly advanced our understanding, a systematic *ab initio* study encompassing energies, radii, electromagnetic properties, and geometric structures across the beryllium isotopes is still lacking. Moreover, the identification of cluster structure and molecular orbitals from the full A-body wave function remains a question.

Recent advancements in nuclear lattice effective field theory (NLEFT) offer promising avenues for such comprehensive investigations. The introduction of wave function matching techniques within NLEFT, combined with state-of-the-art next-to-next-to-next-to-leading order (N^3LO) chiral interactions, has led to remarkable agreement with experimental data across a range of nuclei [45]. Moreover, NLEFT has successfully described the structure of the Hoyle state in ^{12}C [46,47], α-α scattering processes [48], geometric configurations of the ^{12}C spectrum [49], nuclear thermodynamics [50], clustering in hot dilute matter [51], structure factors for hot neutron matter [52], hyperneutron matter [53], and hypernuclei [54]. In this work, we present a systematic *ab initio* study of the p-shell beryllium isotopes using NLEFT with the N^3LO interaction, including energies, radii, electromagnetic properties, and the geometric structures.

Formalism—We use the wave function matching method [45] to mitigate the Monte Carlo sign problem associated with high-fidelity N^3LO chiral interactions. This method unitarily transforms the original Hamiltonian, H, into a new high-fidelity Hamiltonian, H', such that its wave functions match those of a computationally simple Hamiltonian, H^S, up to a given radius. This transformation ensures that the expansion in powers of the difference $H' - H^S$ converges rapidly. For more details see Ref. [45]. For comparison, we also employ a simple SU(4)-symmetric interaction for the study of ^{12}C [49].

In the NLEFT framework [55,56], observables are calculated as

$$\langle O \rangle = \lim_{\tau\to\infty} \frac{\langle \Psi_0 | M^{L_t/2} O M^{L_t/2} | \Psi_0 \rangle}{\langle \Psi_0 | M^{L_t} | \Psi_0 \rangle}, \tag{1}$$

where Ψ_0 is the initial wave function, M is the normal-ordered transfer matrix operator $:e^{-H^S a_t}:$ with temporal lattice spacing a_t, and L_t is the total number of temporal lattice steps.

To study the nuclear geometrical properties, we employ the pinhole algorithm [57] and its perturbative extension [58]. The method samples the positions of A-nucleons, denoted as $\mathbf{n}_i$, on the lattice (spin and isospin indices have been omited) according to the following amplitude

$$Z = \langle \Psi_0 | M^{L_t/2} \rho(\mathbf{n}_1, \mathbf{n}_2, \ldots, \mathbf{n}_A) M^{L_t/2} | \Psi_0 \rangle, \tag{2}$$

where $\rho(\mathbf{n}_1, \mathbf{n}_2, \ldots, \mathbf{n}_A)$ is the normal-ordered product of single-nucleon density operators $\rho(\mathbf{n}_i) = a^\dagger(\mathbf{n}_i) a(\mathbf{n}_i)$. Let $N_{\rm pin}$ represent the total number of sampled pinhole configurations. These configurations can be written as

$$\left\{ \mathbf{N}^{(k)} = \left(\mathbf{n}_1^{(k)}, \mathbf{n}_2^{(k)}, \ldots, \mathbf{n}_A^{(k)} \right) \right\}_{k=1}^{N_{\rm pin}}, \tag{3}$$

where $N_{\rm pin}$ typically reaches several millions for the current study of beryllium isotopes. Each configuration then can be transformed into the A-nucleon center-of-mass (c.m.) coordinate, $\mathbf{r}_i$, [57]:

$$\left\{ \mathbf{R}^{(k)} = \left(\mathbf{r}_1^{(k)}, \mathbf{r}_2^{(k)}, \ldots, \mathbf{r}_A^{(k)} \right) \right\}_{k=1}^{N_{\rm pin}}. \tag{4}$$

To account for the finite nucleon size (0.84 fm) [59], a random Gaussian smearing is applied.

The quadrupole moment for a given configuration can then be calculated as (the denominator required for normalization has been omitted)

$$\langle Q \rangle = e \sum_{k=1}^{N_{\rm pin}} (-1)^{s_k} \sum_{i=1}^{Z} [r_i^{(k)}]^2 \left(3\cos^2\theta_i^{(k)} - 1 \right), \tag{5}$$

with $s_k = 0$ or 1 for the sign due to importance sampling to the absolute amplitude of $|Z|$ [56,57], and the summation is over protons. The reduced transition probability is

$$\langle B(E\lambda; I_1 \to I_2) \rangle = e^2 \sum_{\mu M_2} \left| \sum_{k=1}^{N_{\rm pin}} (-1)^{s_k} \sum_{i=1}^{Z} r_i^\lambda Y_{\lambda\mu}(\hat{\mathbf{r}}_i) \right|^2. \tag{6}$$

The deformation parameters [60] for a given pinhole configuration (k) are

$$a_{20}^{(k)} = \frac{4\pi}{3AR_0^2} \sqrt{\frac{5}{16\pi}} \sum_{i=1}^{A} \left(3[z_i^{(k)}]^2 - [r_i^{(k)}]^2 \right), \tag{7a}$$

$$a_{22}^{(k)} = \frac{4\pi}{3AR_0^2} \sqrt{\frac{15}{32\pi}} \sum_{i=1}^{A} \left([x_i^{(k)}]^2 - [y_i^{(k)}]^2 + i x_i^{(k)} y_i^{(k)} \right), \tag{7b}$$

with $R_0 = 1.2$ fm $A^{1/3}$. The Hill-Wheeler coordinates [61] β, γ can be calculated with

$$a_{20}^{(k)} = \beta^{(k)} \cos\gamma^{(k)}, \qquad a_{22}^{(k)} = \frac{1}{\sqrt{2}} \beta^{(k)} \sin\gamma^{(k)}. \tag{8}$$

By a suitable rotation, the expectation value of $\langle xy \rangle$ vanishes. The statistical average over $N_{\rm pin}$ configurations will give us a deformation distribution for a given state of nucleus. To distinguish it from single determinant deformation, we label it as $\beta_{\rm pin}$ and $\gamma_{\rm pin}$.

Note that the expressions in Eqs. (4)–(7) have no explicit left $\langle L|$ and right $|R\rangle$ states information, they are encoded in

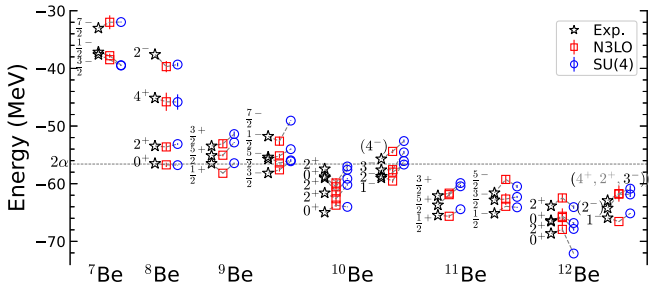

FIG. 1. Low-lying spectrum from ^{7}Be to ^{12}Be calculated by NLEFT using N^{3}LO interaction [45] and SU(4) interaction [49], compared to the data [63–68]. The error bars correspond to 1 standard deviation errors include stochastic errors and uncertainties in the Euclidean time extrapolation. The two α threshhold is denoted by the horizontal dashed line.

Eq. (2). For transition obsevables (6) a multichannel calculation with different bra and ket states will be performed.

Results and discussion—The N^{3}LO interaction described in Ref. [45] and SU(4)-symmetric interaction in Ref. [49] are defined on lattices with spatial spacings $a = 1.32$ and 1.64 fm, respectively, which correspond to momentum cutoffs $\Lambda = \pi/a \simeq 471$ and 377 MeV. Additionally, the temporal lattice spacings for these interactions are defined as $a_t = 0.20$ and $a_t = 0.55$ fm, respectively, for these interactions. We perform our lattice calculation in a periodic cubic box with length $L = 13.2$ fm for the N^{3}LO interaction and 14.8 fm for the SU(4)-symmetric interaction. See Ref. [62] for the details on the configurations of the initial wave functions.

Figure 1 displays the low-lying energy spectra of ^{7}Be to ^{12}Be calculated using NLEFT with the N^{3}LO interaction, compared to experimental data [63–68]. The trends of the theoretical predictions agree with the experimental results, affirming the effectiveness of the N^{3}LO interaction in reproducing both ground and excited states of beryllium isotopes. Numerical challenges such as Euclidean time extrapolation and finite volume effects become more pronounced for excited states [62], making it more difficult to maintain the same level of accuracy as for ground states. Addressing these challenges will require further optimization of computational algorithms and fine-tuning of three-body forces. Despite these challenges, the successful application of NLEFT to beryllium isotopes underscores its potential for accurately capturing the complex dynamics of light nuclei.

It is noteworthy that the simple SU(4)-symmetric interaction [49] also provides an accurate description of most of the states, especailly ^{11}Be. The ground state of ^{11}Be has long posed a challenge to nuclear structure theory due to its inverted parity ordering, where the $1/2^+$ state lies below the $1/2^-$ state, contrary to shell-model predictions [4,39,43]. Using only the SU(4)-symmetric interaction, we successfully reproduce this ordering with high precision: $E(\frac{1}{2}^+) = -64.6(1)$ and $E(\frac{1}{2}^-) = -64.1(1)$ MeV, compared to the experimental values of -65.5 and -65.2 MeV, respectively. This result underscores the importance of many-body correlations in achieving accurate nuclear structure descriptions.

TABLE I. Energies of states in ^{7}Be and ^{10}Be calculated by NLEFT that have not been identified by experiments. For ^{7}Be some results from NCSM calculations [38] are listed for comparison.

	NLEFT, N^{3}LO	NLEFT, SU (4)	NCSM
^{7}Be, $(\frac{3}{2}^+)$	$-30.5(8)$	$-29.9(3)$	-24.7
^{7}Be, $(\frac{1}{2}^+)$	$-28.8(1)$	$-31.9(2)$	-27.8
^{7}Be, $(\frac{5}{2}^+)$	$-26.5(7)$	$-26.5(1)$	
^{10}Be, $A_1^+(3)$	$-56.1(7)$	$-58.4(9)$	

By exploring various configurations, we identify states in beryllium isotopes that have not yet been observed experimentally, as listed in Table I. The existence of positive-parity states in ^{7}Be has been a subject of long-standing debate [69,70]. Using shell-model wave functions with one proton excited to the *sd* shell, our calculations yield lower energies compared to the NCSM results [38].

For ^{10}Be, a three-channel 0^+ calculation with *irrep* A_1^+ projection [71,72] reveals that the ground state is a mixture of $1p_{3/2}$ and $1p_{1/2}$ channels, the second 0^+ state is predominant by *sd* shell, and the third state also comprises a mixture of $1p_{3/2}$ and $1p_{1/2}$. While the 0_2^+ state with *sd*-shell or σ-orbital characteristics is well established [25,42], the nature of the third A_1^+ state remains unclear. Although it could correspond to a 4^+ state, its calculated energy ($-56 \sim -58$ MeV) is significantly lower than the experimental 4_1^+ at -53.2 and the -49 MeV obtained from similar $J_z = 4$ calculations.

Figure 2 displays the charge radii and point matter radii of beryllium isotopes with available experimental data [12,73–75]. Our theoretical results, compared to calculations from AMD [10], FMD [12], and THSR [15–17], agree with experimental values within approximately 6% and follow the same trend. Notably, the halo structure of ^{11}Be is accurately reproduced using the N^{3}LO interaction.

We present the calculated quadrupole moments and transition rates for ^{7}Be to ^{12}Be in Table II. These transition calculations are challenging due to slow convergence in Euclidean time and complex multichannel dynamics [76]. To address this, Euclidean time extrapolation has been employed, see [62]. Our results generally agree with the experimental data, with deviations observed in some cases. Given that electromagnetic observables are highly sensitive to nuclear geometric structures, achieving precise reproduction is inherently ambitious. Many theoretical studies (see Table II and [77–88]) have examined these electromagnetic properties, and we compare their findings in [62]. Additionally, we are developing a new method that combines

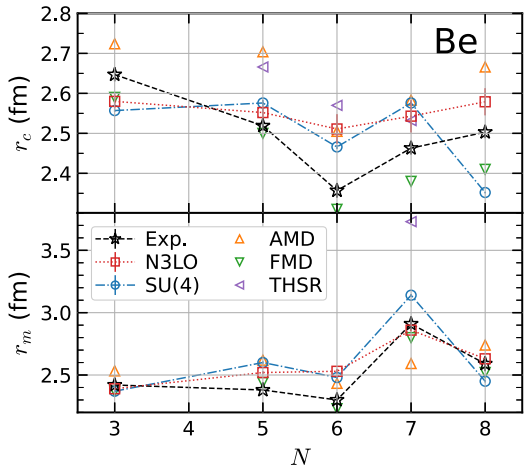

FIG. 2. Radii from ^{7}Be to ^{12}Be calculated by NLEFT using N^{3}LO interaction [45] and SU(4) interaction [49], compared to the data [12,73–75] and other theoretical calculations [10,12,15–17]. For Refs. [10,15,17] proton size, neutron size, and relativistic correction are added. (Upper panel) charge radii; (lower panel) point matter radii.

TABLE II. The quadrupole moment and transition rates of Be isotopes calculated by NLEFT using the N^{3}LO interaction [45] and SU(4) interaction [49], in comparison with experiment. Units for Q and $m(E0)$ are e fm^2, for $B(E1)$ are e^2 fm^2, and for $B(E2)$ are e^2 fm^4.

		SU(4)	N^{3}LO	Exp.
^{7}Be	$E2, \frac{3}{2}^- \to \frac{1}{2}^-$	16.0(2)	15.2(5)	26(6)(3) [91]
^{9}Be	$Q(\frac{3}{2}^-)$	7.3(1)	7.4(1.0)	5.29(4) [92]
	$E1, \frac{1}{2}^+ \to \frac{3}{2}^-$	0.131(3)	0.060(15)	0.136(2) [93]
	$E1, \frac{5}{2}^+ \to \frac{3}{2}^-$	0.045(14)	0.049(5)	0.010(8) [67]
	$E2, \frac{5}{2}^- \to \frac{3}{2}^-$	35.7(1.8)	27.8(1.9)	27.1(2.0) [67]
	$E2, \frac{7}{2}^- \to \frac{3}{2}^-$	11.6(2.5)	5.3(8)	9.5(4.1) [67]
^{10}Be	$E1, 3_1^- \to 2_1^+$	0.026(2)	0.004(3)	0.009(1) [67]
	$E2, 2_1^+ \to 0_1^+$	10.6(4)	8.5(9)	9.2(3) [31]
^{11}Be	$E1, \frac{1}{2}^- \to \frac{1}{2}^+$	0.023(3)	0.038(3)	0.102(2) [94]
^{12}Be	$E1, 0_1^+ \to 1_1^-$	0.049(2)	0.056(26)	0.051(13) [95]
	$E2, 2_1^+ \to 0_1^+$	7.8(1.1)	9.0(3.1)	14.2(1.0)(2.0) [6]

second-order perturbative Monte Carlo [89] with a trimmed sampling algorithm [90] to study transitions involving second 0^+ and 2^+ states using the N^{3}LO interaction.

Recent experimental advancements, such as the collective-flow-assisted nuclear shape-imaging technique introduced by STAR [96], have provided unprecedented insights into the shapes of atomic nuclei, highlighting the need for complementary theoretical approaches. In Fig. 3, we present the probability distributions of the deformation parameters $\beta_{\rm pin}$ and $\gamma_{\rm pin}$ for the beryllium isotopes. This model-independent analysis offers a statistical representation of the relative positions of all nucleons, distinguishing it from traditional energy surface plots based on single Slater determinants. Our results demonstrate that the occupation

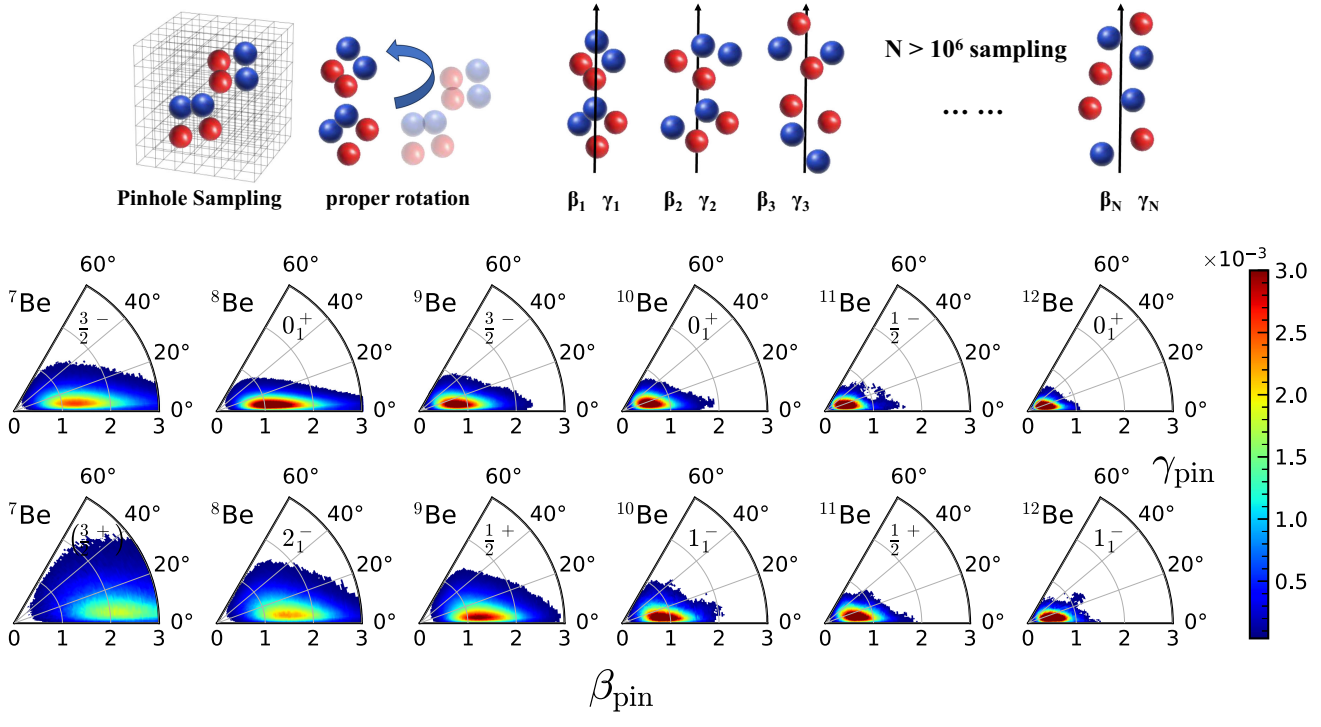

FIG. 3. Probability distribution of the deformation parameter $\beta_{\rm pin}$ and $\gamma_{\rm pin}$ in Eq. (8) through sampling of pinhole configuration by NLEFT using N^{3}LO interaction, with red color representing a higher probability and blue color lower. The third component of total spin is fixed at $J_z = J$.

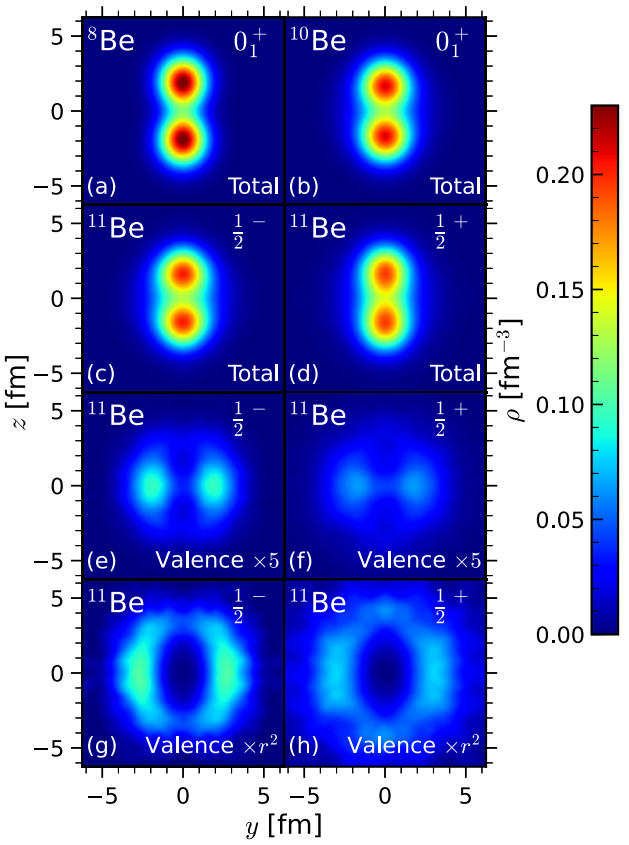

FIG. 4. Intrinsic density at $x = 0$ plane of selected states of beryllium isotopes obtained by NLEFT using N^{3}LO interaction. The third component of total spin is fixed at $J_z = J$. From (a) to (d), the total density of selected nuclear states is shown; from (e) to (f), the valence neutron densities in ^{11}Be are plotted with different scaling.

of different valence neutron orbitals—specifically π or σ orbitals significantly alters the nuclear shape. In particular, valence neutrons occupying σ orbitals lead to more prolate deformations, whereas the occupation of π orbitals results in more spherical shapes. These findings are consistent with the nuclear molecular framework [25,30,34,97].

Finally, we present intrinsic density plots of selected states in beryllium isotopes in Fig. 4. To obtain these intrinsic densities, we adopt the strategy from Ref. [49], which groups the closest two protons and two neutrons and randomly aligns the clusters along the $\pm z$-axis. This method ensures a balanced representation of nuclear shapes, avoiding the overemphasis of any single axis that occurs when aligning configurations based on the principal axis [32,62].

Panels 4(a)–4(d) display the total density for ^{8}Be, ^{10}Be, and ^{11}Be ($1/2^-$ and $1/2^+$ states). ^{8}Be clearly shows a strong two-alpha cluster structure as expected. Adding valence neutrons in ^{10}Be and ^{11}Be slightly diminishes the cluster formation while enhancing the neck region between clusters. Comparing the $1/2^-$ and $1/2^+$ states of ^{11}Be, we observe significantly different shapes: the π-orbital occupation results in a more rounded nucleus, whereas the σ orbital induces a pronounced prolate deformation, consistent with nuclear molecular dynamics in other studies [25,30,34,97].

Panels 4(e)–4(h) illustrate the valence neutron densities, scaled by a constant factor of 5 or by r^2. In panel (e), the π-orbital in ^{11}Be naturally emerges from the N^{3}LO interaction, displaying a distinct distribution. For the $1/2^+$ state in panel (f), one neutron occupies the σ orbital, reducing the π-orbital density. Applying an r^2 scaling in panels (g) and (h) reveals the large spatial extension of the last neutron in the $1/2^+$ state, characteristic of a halo nucleus. This extended distribution aligns with other models [11,25], showing enhanced density around $r \sim 0$ and along the $\pm z$ axis, alongside shell-model *sd* characteristics indicative of a halo structure.

The concept of nuclear molecular orbitals has been extensively discussed in cluster models [25], but it remains less straightforward in the context of *ab initio* calculations. The primary challenge lies in identifying the clusters and valence particles within the full many-body correlated wave function $\Psi(\mathbf{r}_1, \mathbf{r}_2, \ldots, \mathbf{r}_A)$. The current work offers new insights into this task. By performing Monte Carlo sampling of the many-body density operator, the pinhole algorithms provide configurations of the A particle coordinates in space. Furthermore, by grouping the closest 2 protons and 2 neutrons together, the remaining particles are automatically categorized as valence particles.

In the Supplemental Material [62], we describe in detail the grouping algorithm used, and we also explicitly construct a simple model for the π and σ molecular orbitals that is able to reproduce the *ab initio* nucleonic densities seen for the $3/2^-$ and $1/2^+$ states of ^{9}Be as well as the ground states of ^{10}Be, ^{11}Be, and ^{12}Be [62]. This effectively reveals the nuclear molecular orbitals directly from the full wave function $\Psi(\mathbf{r}_1, \mathbf{r}_2, \ldots, \mathbf{r}_A)$, offering an *ab initio* description of these orbitals.

Summary and discussion—We have systematically studied the *p*-shell beryllium isotopes using nuclear lattice effective field theory (NLEFT) with both the N^{3}LO interaction [45] and a simple SU(4)-symmetric interaction [49]. Our calculations for the low-lying spectra, radii, and electromagnetic observables show good agreement with experimental data. We have investigated the halo structure of ^{11}Be, the geometric differences between negative- and positive-parity states, and intrinsic density distributions. By identifying clusters and valence neutrons from the pinhole algorithm, nuclear molecular orbitals, e.g., π and σ orbitals, emerge naturally. These findings demonstrate the efficiency of NLEFT in capturing the intricate dynamics of light nuclei, highlighting the potential of unified *ab initio* approaches in elucidating complex nuclear behaviors such as the nature and details of the molecular orbitals in nuclei with clustering.

Acknowledgments—We are grateful for discussions with Jie Meng and the members of the NLEFT Collaboration. This work is supported in part by the European Research

Council (ERC) under the European Union's Horizon 2020 research and innovation programme (ERC AdG EXOTIC, Grant Agreement No. 101018170), by DFG and NSFC through funds provided to the Sino-German CRC 110 "Symmetries and the Emergence of Structure in QCD" (NSFC Grant No. 11621131001, DFG Grant No. TRR110). The work of S. S. was supported in by the National Natural Science Foundation of China under Grants No. 12435007. The work of U. G. M. was supported in by the CAS President's International Fellowship Initiative (PIFI) (Grant No. 2025PD0022). The work of S. E. is supported in part by the Scientific and Technological Research Council of Turkey (TUBITAK Project No. 123F464). The work of D. L. is supported in part by the U.S. Department of Energy (Grants No. DE-SC0013365, No. DE-SC0023658, No. DE-SC0024586), U.S. National Science Foundation (Grant No. PHY-2310620) and the nuclear computational low-energy initiative (NUCLEI) SciDAC project. The authors gratefully acknowledge the Gauss Centre for Supercomputing e.V. for funding this project by providing computing time on the GCS Supercomputer JUWELS at Jülich Supercomputing Centre (JSC).

[1] E. G. Adelberger, S. M. Austin, J. N. Bahcall, A. B. Balantekin, G. Bogaert, L. S. Brown, L. Buchmann, F. E. Cecil, A. E. Champagne, L. de Braeckeleer *et al.*, Rev. Mod. Phys. **70**, 1265 (1998).
[2] E. G. Adelberger, A. García, R. G. Hamish Robertson, K. A. Snover, A. B. Balantekin, K. Heeger, M. J. Ramsey-Musolf, D. Bemmerer, A. Junghans *et al.*, Rev. Mod. Phys. **83**, 195 (2011).
[3] P. J. Li, D. Beaumel, J. Lee, M. Assié, S. Chen, S. Franchoo, J. Gibelin, F. Hammache, T. Harada, Y. Kanada-En'yo *et al.*, Phys. Rev. Lett. **131**, 212501 (2023).
[4] A. Calci, P. Navrátil, R. Roth, J. Dohet-Eraly, S. Quaglioni, and G. Hupin, Phys. Rev. Lett. **117**, 242501 (2016).
[5] I. Talmi and I. Unna, Phys. Rev. Lett. **4**, 469 (1960).
[6] C. Morse, E. A. McCutchan, H. Iwasaki, C. J. Lister, V. M. Bader, D. Bazin, S. Beceiro Novo, P. Chowdhury, A. Gade, T. D. Johnson *et al.*, Phys. Lett. B **780**, 227 (2018).
[7] J. Chen, J. L. Lou, Y. L. Ye, Z. H. Li, D. Y. Pang, C. X. Yuan, Y. C. Ge, Q. T. Li, H. Hua, D. X. Jiang *et al.*, Phys. Lett. B **781**, 412 (2018).
[8] S. D. Pain, W. N. Catford, N. A. Orr, J. C. Angelique, N. I. Ashwood, V. Bouchat, N. M. Clarke, N. Curtis, M. Freer, B. R. Fulton *et al.*, Phys. Rev. Lett. **96**, 032502 (2006).
[9] A. Navin, D. W. Anthony, T. Aumann, T. Baumann, D. Bazin, Y. Blumenfeld, B. A. Brown, T. Glasmacher, P. G. Hansen, R. W. Ibbotson *et al.*, Phys. Rev. Lett. **85**, 266 (2000).
[10] Y. Kanada-En'yo, Phys. Rev. C **91**, 014315 (2015).
[11] Y. Kanada-En'yo and H. Horiuchi, Phys. Rev. C **66**, 024305 (2002).
[12] A. Krieger, K. Blaum, M. L. Bissell, N. Frommgen, C. Geppert, M. Hammen, K. Kreim, M. Kowalska, J. Kramer, T. Neff *et al.*, Phys. Rev. Lett. **108**, 142501 (2012).
[13] N. Itagaki and S. Okabe, Phys. Rev. C **61**, 044306 (2000).
[14] W. Von Oertzen, Z. Phys. A **354**, 37 (1996).
[15] M. Lyu, Z. Ren, H. Horiuchi, B. Zhou, Y. Funaki, G. Röpke, P. Schuck, A. Tohsaki, C. Xu, and T. Yamada, Eur. Phys. J. A **57**, 51 (2021).
[16] M. Lyu, Z. Ren, B. Zhou, Y. Funaki, H. Horiuchi, G. Röpke, P. Schuck, A. Tohsaki, C. Xu, and T. Yamada, Phys. Rev. C **93**, 054308 (2016).
[17] M. Lyu, Z. Ren, B. Zhou, Y. Funaki, H. Horiuchi, G. Röpke, P. Schuck, A. Tohsaki, C. Xu, and T. Yamada, Phys. Rev. C **91**, 014313 (2015).
[18] Q. Zhao, M. Kimura, B. Zhou, and S. h. Shin, Phys. Rev. C **106**, 054313 (2022).
[19] T. Fukui, J. Phys. G **49**, 055102 (2022).
[20] V. Della Rocca and F. Iachello, Nucl. Phys. **A973**, 1 (2018).
[21] C. Romero-Redondo, E. Garrido, D. V. Fedorov, and A. S. Jensen, Phys. Rev. C **77**, 054313 (2008).
[22] P. Descouvemont, Nucl. Phys. **A699**, 463 (2002).
[23] M. Kimura, T. Suhara, and Y. Kanada-En'yo, Eur. Phys. J. A **52**, 373 (2016).
[24] Y. Funaki, H. Horiuchi, and A. Tohsaki, Prog. Part. Nucl. Phys. **82**, 78 (2015).
[25] W. von Oertzen, M. Freer, and Y. Kanada-En'yō, Phys. Rep. **432**, 43 (2006).
[26] J. Geng, P. W. Zhao, Y. F. Niu, and W. H. Long, Phys. Lett. B **858**, 139036 (2024).
[27] J. Geng, Y. F. Niu, and W. H. Long, Chin. Phys. C **47**, 044102 (2023).
[28] J. P. Ebran, E. Khan, T. Niksic, and D. Vretenar, Phys. Rev. C **90**, 054329 (2014).
[29] J. P. Linares Fernandez, N. Michel, M. Płoszajczak, and A. Mercenne, Phys. Rev. C **108**, 044616 (2023).
[30] J. Carlson, S. Gandolfi, F. Pederiva, S. C. Pieper, R. Schiavilla, K. E. Schmidt, and R. B. Wiringa, Rev. Mod. Phys. **87**, 1067 (2015).
[31] E. A. McCutchan, C. J. Lister, R. B. Wiringa, S. C. Pieper, D. Seweryniak, J. P. Greene, M. P. Carpenter, C. J. Chiara, R. V. F. Janssens, T. L. Khoo *et al.*, Phys. Rev. Lett. **103**, 192501 (2009).
[32] R. B. Wiringa, S. C. Pieper, J. Carlson, and V. R. Pandharipande, Phys. Rev. C **62**, 014001 (2000).
[33] K. Kravvaris and A. Volya, Phys. Rev. Lett. **119**, 062501 (2017).
[34] T. Yoshida, N. Shimizu, T. Abe, and T. Otsuka, Few-Body Syst. **54**, 1465 (2013).
[35] L. Liu, T. Otsuka, N. Shimizu, Y. Utsuno, and R. Roth, Phys. Rev. C **86**, 014302 (2012).
[36] A. E. McCoy, M. A. Caprio, P. Maris, and P. J. Fasano, Phys. Lett. B **856**, 138870 (2024).
[37] M. A. Caprio, A. E. McCoy, P. J. Fasano, and T. Dytrych, Bulgar. J. Phys. **49**, 057 (2022).
[38] M. Vorabbi, P. Navrátil, S. Quaglioni, and G. Hupin, Phys. Rev. C **100**, 024304 (2019).
[39] C. Forssen, P. Navratil, W. E. Ormand, and E. Caurier, Phys. Rev. C **71**, 044312 (2005).
[40] I. Lombardo and D. Dell'Aquila, Riv. Nuovo Cimento **46**, 521 (2023).
[41] B. Gnoffo, S. Pirrone, G. Politi, G. Cardella, E. De Filippo, E. Geraci, C. Maiolino, N. S. Martorana, A. Pagano, E. V. Pagano *et al.*, Front. Phys. **10**, 1061633 (2022).
[42] Y. Kanada-En'yo and H. Horiuchi, Front. Phys. (Beijing) **13**, 132108 (2018).

[43] H. T. Fortune, Eur. Phys. J. A **54**, 51 (2018).
[44] M. Freer, H. Horiuchi, Y. Kanada-En'yo, D. Lee, and U. G. Meißner, Rev. Mod. Phys. **90**, 035004 (2018).
[45] S. Elhatisari, L. Bovermann, Y. Z. Ma, E. Epelbaum, D. Frame, F. Hildenbrand, M. Kim, Y. Kim, H. Krebs, T. A. Lähde *et al.*, Nature (London) **630**, 59 (2024).
[46] E. Epelbaum, H. Krebs, D. Lee, and U.-G. Meissner, Phys. Rev. Lett. **106**, 192501 (2011).
[47] E. Epelbaum, H. Krebs, T. A. Lahde, D. Lee, and U.-G. Meißner, Phys. Rev. Lett. **109**, 252501 (2012).
[48] S. Elhatisari, D. Lee, G. Rupak, E. Epelbaum, H. Krebs, T. A. Lähde, T. Luu, and U.-G. Meißner, Nature (London) **528**, 111 (2015).
[49] S. Shen, S. Elhatisari, T. A. Lähde, D. Lee, B. N. Lu, and U.-G. Meißner, Nat. Commun. **14**, 2777 (2023).
[50] B. N. Lu, N. Li, S. Elhatisari, D. Lee, J. E. Drut, T. A. Lähde, E. Epelbaum, and U.-G. Meißner, Phys. Rev. Lett. **125**, 192502 (2020).
[51] Z. Ren, S. Elhatisari, T. A. Lähde, D. Lee, and U.-G. Meißner, Phys. Lett. B **850**, 138463 (2024).
[52] Y. Z. Ma, Z. Lin, B. N. Lu, S. Elhatisari, D. Lee, N. Li, U.-G. Meißner, A. W. Steiner, and Q. Wang, Phys. Rev. Lett. **132**, 232502 (2024).
[53] H. Tong, S. Elhatisari, and U. G. Meißner, Sci. Bull. **70**, 825 (2025).
[54] F. Hildenbrand, S. Elhatisari, Z. Ren, and U.-G. Meißner, Eur. Phys. J. A **60**, 215 (2024).
[55] D. Lee, Prog. Part. Nucl. Phys. **63**, 117 (2009).
[56] T. A. Lähde and U.-G. Meißner, Lect. Notes Phys. **957**, 1 (2019).
[57] S. Elhatisari, E. Epelbaum, H. Krebs, T. A. Lähde, D. Lee, N. Li, B. n. Lu, U.-G. Meißner, and G. Rupak, Phys. Rev. Lett. **119**, 222505 (2017).
[58] B. N. Lu, N. Li, S. Elhatisari, D. Lee, E. Epelbaum, and U. G. Meißner, Phys. Lett. B **797**, 134863 (2019).
[59] Y. H. Lin, H. W. Hammer, and U.-G. Meißner, Phys. Rev. Lett. **128**, 052002 (2022).
[60] P. Ring and P. Schuck, *The Nuclear Many-Body Problem* (Springer Science & Business Media, 2004).
[61] D. L. Hill and J. A. Wheeler, Phys. Rev. **89**, 1102 (1953).
[62] See Supplemental Material at http://link.aps.org/supplemental/10.1103/PhysRevLett.134.162503 for additional numerical details and a toy model of molecular orbitals.
[63] W. Liu, J. L. Lou, Y. L. Ye, S. M. Wang, Z. W. Tan, Z. H. Li, Q. T. Li, H. Hua, X. F. Yang, J. Y. Xu *et al.*, Phys. Rev. C **105**, 034613 (2022).
[64] M. Wang, W. J. Huang, F. G. Kondev, G. Audi, and S. Naimi, Chin. Phys. C **45**, 030003 (2021).
[65] J. H. Kelley, J. E. Purcell, and C. G. Sheu, Nucl. Phys. **A968**, 71 (2017).
[66] J. H. Kelley, E. Kwan, J. E. Purcell, C. G. Sheu, and H. R. Weller, Nucl. Phys. **A880**, 88 (2012).
[67] D. R. Tilley, J. H. Kelley, J. L. Godwin, D. J. Millener, J. E. Purcell, C. G. Sheu, and H. R. Weller, Nucl. Phys. **A745**, 155 (2004).
[68] D. R. Tilley, C. M. Cheves, J. L. Godwin, G. M. Hale, H. M. Hofmann, J. H. Kelley, C. G. Sheu, and H. R. Weller, Nucl. Phys. **A708**, 3 (2002).
[69] D. Piatti, T. Chillery, R. Depalo, M. Aliotta, D. Bemmerer, A. Best, A. Boeltzig, C. Broggini, C. G. Bruno, A. Caciolli *et al.*, Phys. Rev. C **102**, 052802(R) (2020).
[70] J. J. He, S. Z. Chen, C. E. Rolfs, S. W. Xu, J. Hu, X. W. Ma, M. Wiescher, R. J. Deboer, T. Kajino, M. Kusakabe *et al.*, Phys. Lett. B **725**, 287 (2013).
[71] R. C. Johnson, Phys. Lett. **114B**, 147 (1982).
[72] B. N. Lu, T. A. Lähde, D. Lee, and U.-G. Meißner, Phys. Rev. D **90**, 034507 (2014).
[73] W. Nortershauser, D. Tiedemann, M. Zakova, Z. Andjelkovic, K. Blaum, M. L. Bissell, R. Cazan, G. W. F. Drake, C. Geppert, M. Kowalska *et al.*, Phys. Rev. Lett. **102**, 062503 (2009).
[74] A. V. Dobrovolsky, G. A. Korolev, A. G. Inglessi, G. D. Alkhazov, G. Colò, I. Dillmann, P. Egelhof, A. Estradé, F. Farinon, H. Geissel *et al.*, Nucl. Phys. **A989**, 40 (2019).
[75] I. Tanihata, H. Savajols, and R. Kanungo, Prog. Part. Nucl. Phys. **68**, 215 (2013).
[76] M. A. Caprio, P. J. Fasano, and P. Maris, Phys. Rev. C **105**, L061302 (2022).
[77] T. Heng, J. P. Vary, and P. Maris, Phys. Rev. C **95**, 014306 (2017).
[78] M. Pervin, S. C. Pieper, and R. B. Wiringa, Phys. Rev. C **76**, 064319 (2007).
[79] S. Pastore, S. C. Pieper, R. Schiavilla, and R. B. Wiringa, Phys. Rev. C **87**, 035503 (2013).
[80] Y. Kanada-En'yo, Phys. Rev. C **93**, 024322 (2016).
[81] S. C. Pieper, K. Varga, and R. B. Wiringa, Phys. Rev. C **66**, 044310 (2002).
[82] K. Arai, P. Descouvemont, D. Baye, and W. N. Catford, Phys. Rev. C **68**, 014310 (2003).
[83] T. Myo, M. Lyu, Q. Zhao, M. Isaka, N. Wan, H. Takemoto, and H. Horiuchi, Phys. Rev. C **108**, 064314 (2023).
[84] P. Descouvemont and N. Itagaki, Prog. Theor. Exp. Phys. **2020**, 023D02 (2020).
[85] J. N. Orce, T. E. Drake, M. K. Djongolov, P. Navratil, S. Triambak, G. C. Ball, H. Al Falou, R. Churchman, D. S. Cross, P. Finlay *et al.*, Phys. Rev. C **86**, 041303(R) (2012).
[86] M. Dan, R. Chatterjee, and M. Kimura, Eur. Phys. J. A **57**, 203 (2021).
[87] M. Dufour, P. Descouvemont, and F. Nowacki, Nucl. Phys. **A836**, 242 (2010).
[88] Y. Kanada-En'yo and H. Horiuchi, Phys. Rev. C **68**, 014319 (2003).
[89] B.-N. Lu, N. Li, S. Elhatisari, Y.-Z. Ma, D. Lee, and U.-G. Meißner, Phys. Rev. Lett. **128**, 242501 (2022).
[90] C. Hicks and D. Lee, Phys. Rev. Res. **5**, L022001 (2023).
[91] S. L. Henderson, T. Ahn, M. A. Caprio, P. J. Fasano, A. Simon, W. Tan, P. O'Malley, J. Allen, D. W. Bardayan, D. Blankstein *et al.*, Phys. Rev. C **99**, 064320 (2019).
[92] N. J. Stone, At. Data Nucl. Data Tables **111–112**, 1 (2016).
[93] C. W. Arnold, T. B. Clegg, C. Iliadis, H. J. Karwowski, G. C. Rich, J. R. Tompkins, and C. R. Howell, Phys. Rev. C **85**, 044605 (2012).
[94] E. Kwan, C. Y. Wu, N. C. Summers, G. Hackman, T. E. Drake, C. Andreoiu, R. Ashley, G. C. Ball, P. C. Bender, A. J. Boston *et al.*, Phys. Lett. B **732**, 210 (2014).
[95] H. Iwasaki, T. Motobayashi, H. Akiyoshi, Y. Ando, N. Fukuda, H. Fujiwara, Z. Fülöp, K. I. Hahn, Y. Higurashi, M. Hirai *et al.*, Phys. Lett. B **491**, 8 (2000).
[96] M. I. Abdulhamid *et al.*(STAR Collaboration), Nature (London) **635**, 67 (2024).
[97] Y. Kanada-En'yo, M. Kimura, and A. Ono, Prog. Theor. Exp. Phys. **2012**, 01A202 (2012).